Functional Nanostructured Materials (including low-D carbon)

Conformable Holographic Photonic Ink Sensors Based on Adhesive Tapes for Strain Measurements

Bader AlQattan, David Benton, Ali K. Yetisen, and Haider Butt

ACS Appl. Mater. Interfaces, **Just Accepted Manuscript** • DOI: 10.1021/acsami.9b08545 • Publication Date (Web): 18 Jul 2019

Conformable Holographic Photonic Ink Sensors Based on Adhesive Tapes for Strain Measurements

Bader AlQattan,[1,] David Benton,[2] Ali K. Yetisen,[3] Haider Butt[4,*]*

[1]School of Engineering, University of Birmingham, Birmingham B15 2TT, UK

[2]Aston Institute of Photonics Technologies, Aston University, Birmingham, B4 7ET, UK

[3]Department of Chemical Engineering, Imperial College London, London SW7 2AZ

[4]Department of Mechanical Engineering, Khalifa University, Abu Dhabi 127788, UAE

[*] bxa301@alumni.bham.ac.uk; haider.butt@ku.ac.ae

Abstract

Buildings, bridges, and aircrafts are frequently exposed to fluctuation loads which could start with a fine crack that instantly lead to unpredictable structure failures. The stationary strain sensors can be utilized, but they are costly and only detect limited deformations forms and sizes. Here, we fabricated photonic strain sensors on adhesive tapes which can provide real-time monitoring of irregular surfaces. Holographic interference patterning was used to produce non-linear curved nanostructures of 1D of (900 nm × 880 nm) and 2D from black dye film on a robust uniform adhesive layer and heat resistance tape. The patterned structure of the black dye was stable in broad pH environments. Diffracted light from the curved nanostructure detected the signal during structural damage, shift or material tear of 5 με at less than 1.3 N cm^{-2}. Additionally, the 2D nanostructure detected a surface change from x or y axis. Tilting the 1D structure within the range of 0.3° to 14.2° provided visible wavelength changes under broadband light to reveal early deflection signs. The curved nonpatterns could be also used for

transferable holographic symbol design. Photonic nanopatterns on an adhesive tape could be used as a rapid response, conformable, lightweight, and low-cost dynamic strain sensor.

KEYWORDS: Holography; laser ablation; diffraction gratings; surface wettability; strain sensing

Introduction

Buildings can be damaged during their operational lifetime due to unforeseen foundation settlement, design error, or seismic events. Metals, concrete, and composite materials are the main supporting structures for buildings, bridges, and aircrafts[1-3]. High cost associated with wireless strain sensors limits continuous observation of the large constructions and unconventional geometries. There are many complex systems, with large and non-planar surfaces that require vigorous alert systems to prevent any catastrophic damage[1, 4]. Complex and wrinkled surfaces may affect the fabrication of micro- and nano-scale devices. Non-planar displacement and the shear traction behavior up to 10 cm often leads to lengthy change but not considered a deformation for many devices[5]. For example, stalactite straws growing beneath concrete may destabilize a building's structure. Humidity, low air circulation, CO_2 concentration, variation in pH can accelerate the growth of stalactite straws, which degrade the concrete texture [6]. For example, in the United States there are more than 600,000 bridges which limits continuous inspections due to the growing costs. One in four bridges are considered structurally inadequate for use, which raise a public safety concern. A bridge deck should be examined if strain value increases from 60 to 80 με, where the structure would develop a fatigue when the strain reaches 150 με.[3] Tension indicators are highly desirable for monitoring and recording health conditions in civil engineering, aerospace, and human interface applications.

MicroStrain miniature sensors use nodes in a bridge structure for wireless discrete placement to measure structure problems such as vibration, load, strain, corrosion, displacement, and tilt. They can measure bending strains of ±400 μm. Similarly, non-destructive testing (NDT), which use a robot to inspect bridge cables, requires a high-voltage X-ray tube and gamma rays for detecting wire cable damage at every 30 cm [3, 7]. Some aircraft structures are made of carbon fibre as a light material, but unpredictable discrete events can cause structural delamination. In addition, most modern aircrafts are made of a composite material structure which can have complex failures, such as resin cracking, fibre breakout, and disjointing. These failure mechanisms are hard to detect and require frequent manual inspections (imaging), significantly increasing operating costs of airlines [8, 9]. Fibre Bragg gratings (FBG) have been used in airplanes and other engineering applications to measure tension load by monitoring light wavelength shifts as a reliable technique. Attaching FBG under the composite skin and stiffener allows monitoring the structural stability of large aircrafts. However, this measurement technique could interoperate a failure occurrence close to the localized area and the minimum length of FBG to produce accurate measurements is at least 6 mm[10]. It can respond to stretch/failure which is restricted to the glued zone of FBG wear. It also has weak deformation capability (25 kN), a narrow and uniform strain failure measurement range (< 2%), and 1 mm m^{-1} resolution [10-12]. Some transducer strain sensors are only able to measure deformation (mm scales) and subject to inconsistency on unconventional surfaces [7, 13, 14] . Piezoresistive strain sensing is flexible, require low power consumption, and is lightweight strain sensors; nevertheless they require complex installation and wiring at point-of-testing sites [4, 15, 16]. It is highly desirable to develop low-cost, rapid, and wireless sensors for structure strain monitoring.

Feasible and highly-responsive strain sensors can be fabricated from optical nanostructures because they enable the control of the light direction [17, 18]. A non-linear nanostructure could

provide a strong non-linear response especially in unconventional surfaces[18-20]. An embedded nanostructure on a commercial adhesive tape would produce a low cost and flexible strain sensor conformable to any surface. Nevertheless, integrating nanoscale features over commercial tape represents an essential challenge. Convential nanofabrication methods are able to form optical structures; however, they are costly and time consuming [21-23]. Methods such as contact stamping, micro molding, E-beam processing, and ultrashort laser pulse lithography can be used to fabricate nanostructures on a tape [24-26]. Nevertheless, these fabrication methods require complex setups, high-energy supplies, multiple steps, high-cost equipment, and long fabrication times [22, 27, 28]. In addition, there are many laser interference systems that are able to produce nanostructures [29]; however, they may damage the thin plastic substrates due to their highly-intense pulse beam energy [30].

Here, optical nanostructures were rapidly produced at low cost by a holographic laser ablation. Black dye deposited on a commercial adhesive tape was patterned by ablative interference fringes using direct laser interference patterning (DLIP). Holographic DLIP in Denisyuk reflection mode generated a Fresnel zone plate (FZP) and curved grating (CG) 1D/2D on the tape without damaging the substrate [31, 32]. Additional samples were fabricated by changing the samples' tilt angle range between 5° and 35° at different incident positions on a concave mirror to study the light diffraction effects with monochromatic light. The wettability of 1D and 2D nanostructures were characterized. The nanostructures on the tape were examined for dynamic sensing applications.

Results

Holographic fabrication of FZP and curved grating nanostructures

Glass slides were coated with black dye which acted as a recording medium to obtain accurate and reliable measurements. This dye was selected because it can absorb the interference pattern from a laser beam to obtain a well-defined nanostructure [33]. The black dye had a long-term durability up to five years. The thickness of the black dye on the substrate was measured to be 915 nm (Supporting Information Figure S1) [34, 35]. Figure 1a illustrates the setup diagram of the Denisyuk ablation mode to fabricate holographic structures on the recording medium. Initially, the laser beam was directed by a dielectric mirror to eliminate harmonic components from the laser beam, then it was guided to a plane mirror toward two sets of mirrors. The laser beam was directed to the first set by the plane mirrors toward the black dye to pass the recording medium and was reflected from the centre of a concave mirror. The reflected beams from the centre point of the concave mirror formed a focal point (f_c) at 5.0 cm (Eq. 1). The incident and returning laser beams interfered in the black dye to ablate the localized regions on the medium before reaching the focal point (Figure 1b). Due to the concave mirror having a surface at 3.1 mm gradually decreased to the deepest point with a difference of 100 μm, the reflected beam was modulated into a quadruple amplitude wave which ablated different circular periodicities at the exposed region on the dye. A quadruple amplitude wave are considered as non-linear waves, which interfer with the incoming waves[36]. As a result, the ablation produced a FZP structure (Figure 1c)[37]. In the second laser beam exposure process, the laser beam was directed to the edge of the concave mirror, so part of the incident laser beam was reflected from one edge of the concave surface. The quadruple reflected laser profile ablates part of the localized region on the black dye medium to form a CG as a set of semi-circles (Figure 1d).

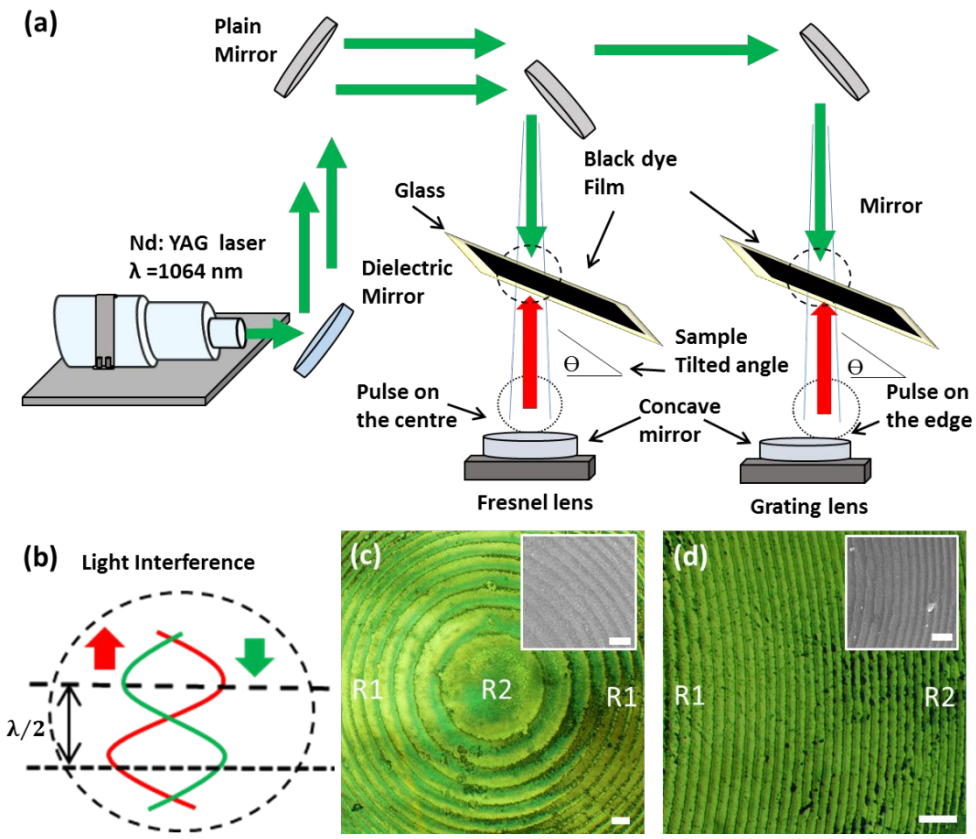

Figure 1. Fabrication of Fresnel lens and distorted patterns of nanosecond DLIP in holographic Denisyuk reflection mode. (a) Nd:YAG laser beam (1064 nm, 3.5 ns) was guided by a dielectric mirror and passed to a set of mirrors through black dye on a glass slide reflected back from (b) laser interference pattern. The centre of the concave mirror (centre pulse (CP); (c) optical image of the fabricated Fresnel lens plate. The second set of mirrors: exposure from the side of the concave mirror (side pulse (SP)); (d) optical radial structure. The insets in (c,d) show SEM images. (Scale bars=100 μm)

Both structures were gratings resulting from the laser interference produced from various regions of the concave mirrors which produced non-linear structures [36, 38-40].

$$f_c = \frac{1}{2} r_c \qquad \text{(Eq. 1)}$$

where r_c is the radius of curvature. Both structures of the concave mirror. The interference of the laser ablation process resulted from two beams. The interference developed from the maximum energy of the incident electric laser wave E_I and reflected electric laser wave E_R is:

$$E^2=E_I{}^2+E_R{}^2+2E_IE_R\cos(\alpha_R-\alpha_I) \quad \text{(Eq. 2)}$$

where λ , x, ω, and t represent the laser wavelength, axis plane, angular frequency and time, respectively. k is the magnitude of the grating vector or the propagation number and can be calculated by $k = 2\pi/\lambda$. The separation of space and phase is defined by $\alpha(x, \varepsilon) = -(kx+\varepsilon)$. The phase difference is represented by $\delta=(\alpha_R-\alpha_I)=2\pi/\lambda(x_1-x_2)$ [41].

The holographic DLIP has produced the FZP and radial structures by arranging the samples' angle at 0° from the incident during the interference. The differences in the phase grating results in different spacings of the photonic structures. Optical microscopy was used to measure the average large structure (R1) and the average smallest periodicity structure (R2) in samples (spacing in central and side regions labelled in Figure 1c-d). The centre pulse (CP) produced the symmetric FZP structures and it had no structure at the midpoint which was considered as R2 with zero periodicity. Figure 2a shows the structure spacing of R1= 12.1μm. On the other hand, the side pulse (SP) structure at 0° showed the spacing of R1= 9 μm centrally, changing to the smallest spacing of R2= 5.6 μm in the outer regions (Figure 2b). Changing the samples' exposure angle (Θ) on the holographic DLIP allowed decreasing of the structure spacing (Λ) as varying tilt angles (5°-35°) [42]. The geometry of the FZP changed after changing the sample tilt angle to 5°, distorting the full circle as the SP structure. Increasing the sample, tilt angle also decreased the periodicities of the structure (Figure 2c). While the same exposure angle of the SP decreased the curve structure and the spacing (Figure 2d). In addition, the resulting difference of the structural spacing of (R1 and R2) for both laser pulses (CP and SP) became close at ~25° (Figure 2e-f). The microscopy images of the CP and SP patterning structures are provided in (Supporting Information Figure S2-3). Eq. 3 was used to estimate

the theoretical mean values of the structural spacing with the exception of 0° tilt angle exposure. The CP structures' mean values were closer to the theoretical values than the SP structures' because the concave mirror surface changed gradually from the centre to the edge. While the SP nanostructures started from a side region of the uneven surface to produce smaller spacing than the CP structure. Both laser reflection positions of CP and SP periodicity were compared with the theoretical spacing (Figure 2g). The experimental and theoretical structures' spacings are provided in (Table 1). Light transmission measurements were conducted on the structures to study the space-light interactions (Figure 2h-i).

$$\Lambda = \frac{\lambda}{2sin\,(\theta)} \qquad \text{(Eq. 3)}$$

Table 1. Periodicity measurement black dyes based on the changing exposure angle; C: pulse on the centre; S: side pulse; R1: smallest regen grating; R2: largest regen grating; Theo: theoretical spacing.

Tilt ang .(°)	C-R1 (µm)	C-R2 (µm)	S-R1 (µm)	S-R2 (µm)	Theo. (µm)
0	0	12.1	9.0	5.6	-
5	7.1	4.9	3.57	3.2	6.1
10	3.52	2.95	2.55	2.2	3.06
15	2.1	1.76	1.74	1.63	2.06
20	1.65	1.5	1.32	1.23	1.56
25	1.23	1.16	1.17	1.12	1.26
30	1.05	1.0	0.96	1.00	1.06
35	0.92	0.9	0.90	0.88	0.923

On-axis exposure using the curved mirror produced circular interference patterns. The holographic properties of the nanofabrication pattern resembled those of a FZP, forming an on-axis diffraction focus beyond the sample with a focal length determined by the radial scale of the pattern. The off-axis exposure produces curved interference patterns and hence curved gratings. Measured transmission intensities decreased as the structure periodicity became smaller. The produced patterns were non-linear structures.

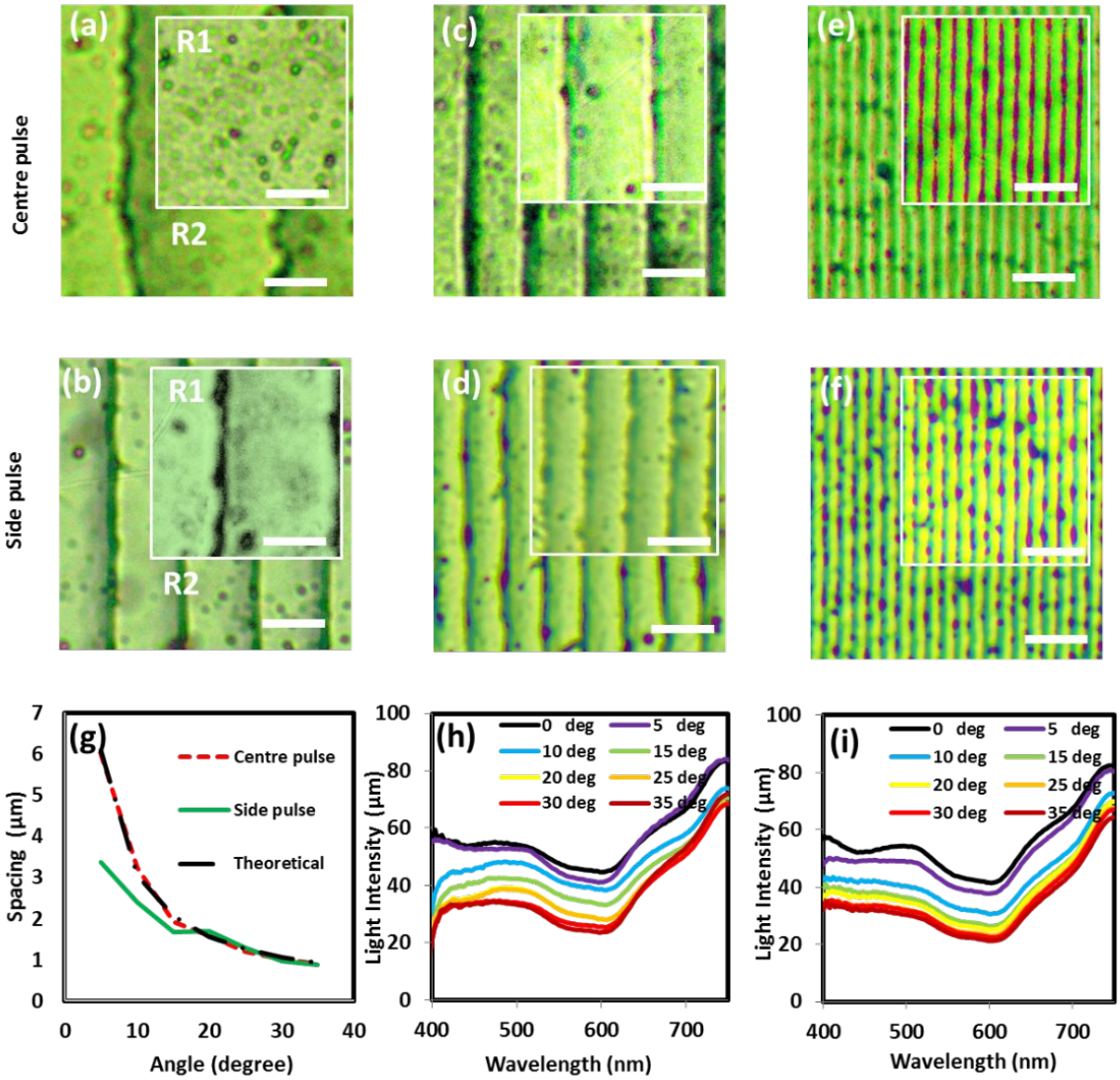

Figure 2. Optical microscopy images showing surface grating nanostructures fabricated by holographic DLIP reflection from the centre and the side of a concave mirror. The effect of changing the laser amplitude due to the reflection and samples' tilt angle on the structures' spacing (the smallest region R1 - the largest region R2 periodicities): (a) 0° (0 μm-12.1 μm); (b) 0°(9 μm-5.6 μm); (c)5° (7.1 μm-4.9 μm); (d) 5° (3.44 μm-3.39 μm); (e) 25° (1.23 μm-1.16 μm); (f) 25° (1.17 μm-1.12 μm). Tilt angle effect on structures' spacing of (g) centre, side pulse structures and theoretical values; (h) transmission on CP structures ;(i) transmission on SP structures. Scale bars = 5 μm.

Optical characterization of the structures

Laser illuminations from three monochromatic light sources blue, green and red wavelengths (450 nm, 532 nm and 635 nm) were used to characterize the patterned structures. The red laser beam illumination (635 nm) on the nanopatterns was used as the main diffraction analysis because it has a long wavelength to generate the largest diffraction angles [17, 40, 43]. The spacing produced at various tilt exposure angles 5° to 35° influenced the diffraction angles to increase for both CP and SP pattern structures [17, 18, 34]. The diffraction was asymmetric with one side diffraction intensity being higher in the first order than the other one in all the structures (Figure 3a-b). The positive orders were less intense because the diffraction was affected by the direction of the curved structures, producing highly intense focal points (f_o) on one side and defocused low intensity spots on the other side [19].

Geometrical theory for diffraction (GTD) was used to simulate 635 nm illumination beam from 5° to 35° tilt angle patterned structure (Figure 3c). In addition, the light intensity reduced as the diffraction angle increased because the structure spacing reduced [19, 38, 39] . The intensity of the CP structures was higher than the SP structures, especially in the larger spacings. Moreover, there were more diffraction points at the CP structure than that of the SP structure. On the other hand, the diffraction angle of the SP structure was higher than that of the CP structure. The difference in the intensity and the diffraction angle also originated from the size of the periodic spacing (Table 1). The experimental diffraction graphs of the CP and SP patterning structures are provided in (Supporting Information Figure S4-5). The diffraction angle of the first order (focal point) can also be estimated based on the periodicity size (Eq. 4-5) and the theoretical and experimental diffraction point is presented in (Supporting Information Table 2).

$$\Lambda = \frac{\lambda m}{sin\,(\alpha)} \qquad \text{(Eq. 4)}$$

$$f_o = \frac{r^2}{2mW} \qquad \text{(Eq. 5)}$$

where the m, α, f_o, r and W are the order number, diffraction angle, focal point, radii of the grating aperture and defocused power [19, 38, 44]. In addition, the diffractions of the CP and SP at 0° had different behaviors. The CP structures of FZP resulted in one diffraction point (f_z) based on a full symmetric circle structure (Figure 3d) (Eq. 6)[45, 46]. Similarly, the SP structures focused on the centre axis (Figure 3e). Although, it has many diffraction points, none of them can be as focused as the one on the centre. The extra diffraction points could also be approximated by Eq. 4. When the exposure angle was changed to 5°, both the patterned structures focused light in the first order (Figure 3f-g). Although the zero order seemed to have higher intensity than the first order, the highest intensity would shift. Further analysis is considered for 25° CP and SP structures by the three laser wavelengths.

$$f_z = \frac{r^2}{m\lambda} \quad \text{(Eq. 6)}$$

The diffraction angle of the shorter wavelength was less than for the longer wavelength [42]. However, the short wavelength illumination (450 nm) resulted in higher intensity than the 532 nm and 635 nm for both patterned structures (Figure 3h-i). The spacing and the shape of the CP and SP structures influenced the diffraction angles and intensity to make one side focus and the other defocus; although the diffraction intensity of the CP structures was higher than that of the SP structures. In addition, if the exposure angle was at 0°, the highest intensity point was always in the centre while the wavelength of the illumination affected the diffraction angle and intensity.

Focusing Analyses of Photonic Structures

The 25° tilted samples of the CP and SP structures were selected with close agreement between the diffraction and the structures' spacing. Using a white screen arranged at the first distance of 18 cm from both the samples and maintaining an image distance at 20 cm, the screen's

distance was decreased by 3.0 cm in six steps. The last step's distance was 1.0 cm as the closest possible point to the sample. Although the images of the first order diffraction spots moved closer to 0 order, all spots moved along one diffraction angle, which was 31° for the CP and 32° for the SP structure (Figure 4a-b). The spot size of the diffraction points decreased as they moved closer to the illumination source. The light intensities of the spots were the lowest at 18 cm in the both samples and increased as they moved closer to the laser illumination source. However, the CP and SP structures provided the highest intensity at 3.0 cm distance at the focused point, then decreased at 2.0 cm from the samples. The SP structure's intensity was higher than the CP structure between 2.0 cm and 3.0 cm because of the subtle difference in the spacing (Figure 4c).

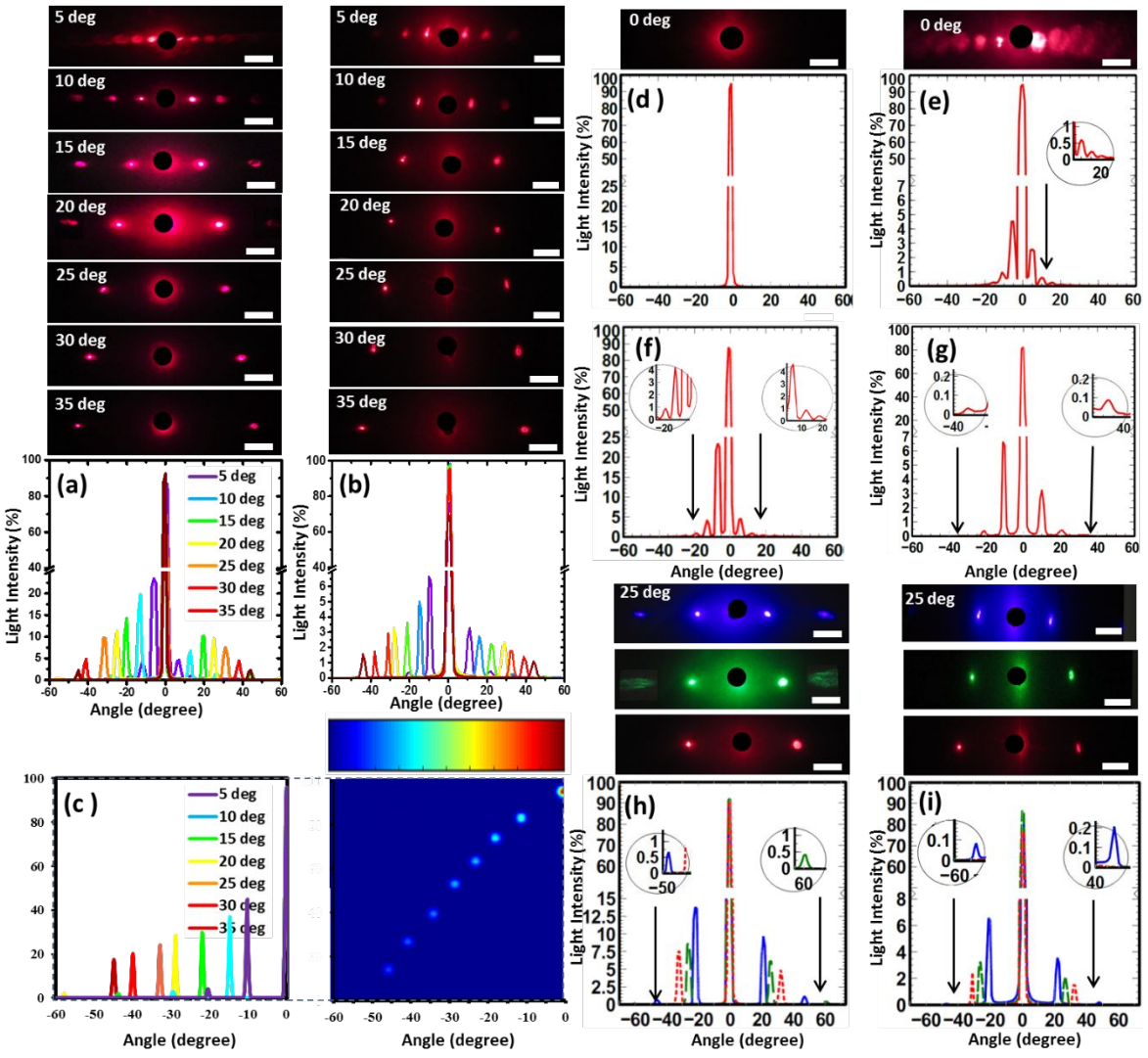

Figure 3. Experimental diffraction analyses of nanostructures with varying periodicities produced at tilt angle of 5°-35° via central pulse (a); and side pulse (b). (c) Simulated diffraction of the patterned structure. Diffraction from 0° samples with (d) symmetric FZP circles and (e) asymmetric curve structures. Red laser illumination on a 5° (f) centre structure; (g) side structure. Diffraction results for 450 nm, 532 nm, and 635 nm wavelengths with 25° tilt angle sample (h) centre pulse; (i) side pulse; scale bar = 5 cm.

Another structure was used to add analyses of focused diffraction intensity (non-linear structure) to show the maximum intensity shifting from zero order to first order [18, 19, 40]. The 5° tilt exposed structure of the CP has been used as one with the highest diffraction points as compared to the other structures. The diffraction images were projected on a screen and analyzed. The intensity of 0 order was low at 18 cm screen distance. The first order (-1) reached the maximum intensity at 12 cm distance; however, the intensity decreased as the screen was brought closer to the structure (Figure 4d-e). Usually in light diffraction, the zero order is the highest intensity but the curve structure able to increase the highest intensity on the first order. Increase and decrease light intensity represents the focus point. A comparison between the negative and positive diffraction intensity points was added to show the total change of diffraction intensity at every point at different distances (Figure 4f-g).

The CP and SP structures at 25° showed equal and low diffraction intensities in the first order at 18 cm distance, then reached maximum diffraction intensity around 2-3 cm at the focused points. In the standard diffraction gratings, there were diffraction orders at angles determined by the average grating spacing. The curved nature of the grating added focal power, positive focussing to the negative orders and negative defocussing to the positive order. The amount of focal power scaled with the order number, hence the +2 order focussed more intensely than the +1 order. In addition, the carved nanostructure was influenced by the size of

the structure to create the maximum intensity at the focus point; which can be used as a highly-intense signal to detect any change of movement or surface shift.

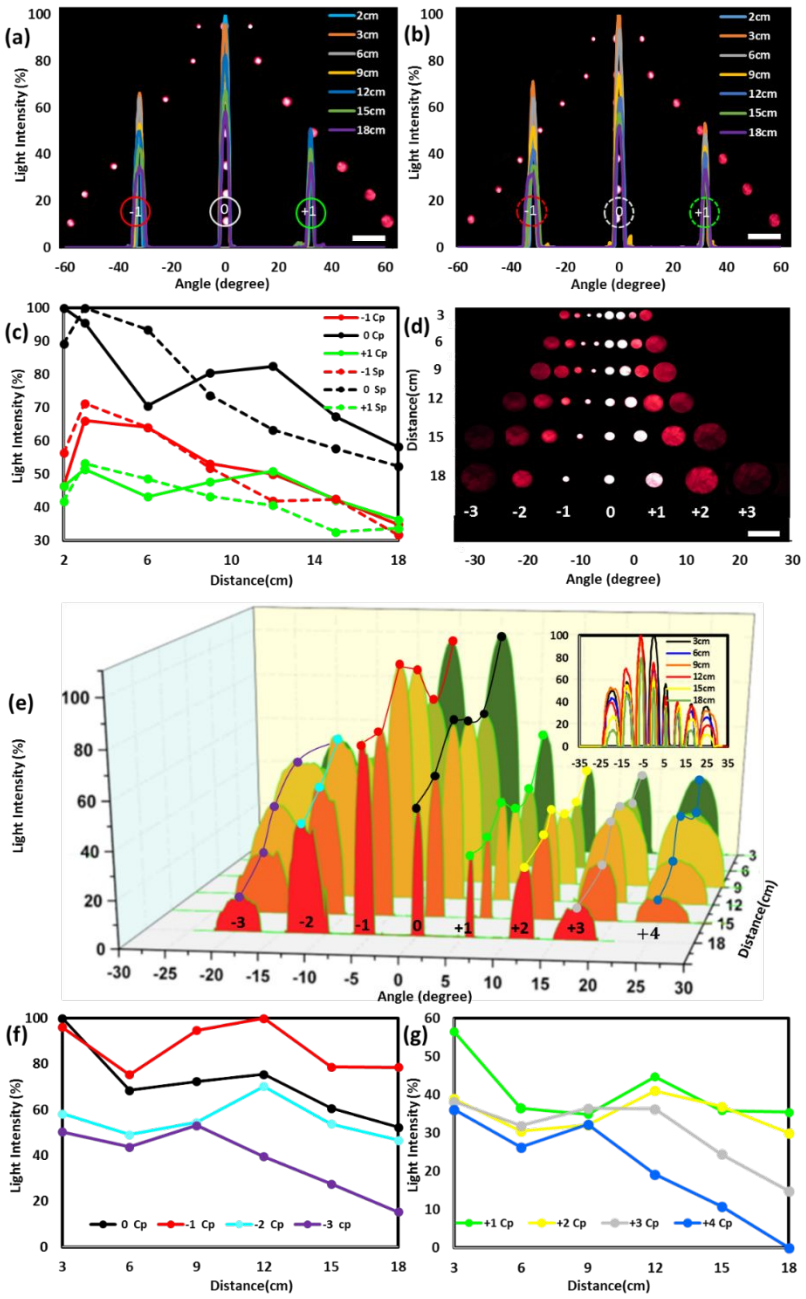

Figure 4. Changing distance of the measured diffraction patterns from 25° tilt angle samples showing the focussing effects of the curved structure focusing to the left and defocusing to the right. Intensity at varying screen distance from the diffraction structure. (a-b) central pulse structure and side pulse structure. (c) Two pulse structure comparison. Changing screen distance of center pulse of 5° to sample tilt angle**.** (d) Image of diffraction at different distances.

Red laser illumination for 5° tilt angle sample. (e) Graph for changing distance and resultant diffraction intensity ;(f) Left side of diffraction points; and (g) right side diffraction points. Scale bar = 5 cm.

Diffraction Spectra Measurements

A goniometer setup was used to measure the angle-resolved diffraction efficiency. The setup was able to measure the rainbow diffraction wavelengths from the photonic structures, as it moved on the motorized rotated stage (Figure 5a). The diffraction rainbow covered the wavelengths range of 400-800 nm. The samples were placed about 17 cm from the spectrometer detector. The length measurements were based on placing a screen at 35 cm away from the diffraction samples. The broadband white light showed different responses when transmitted through both the CP and SP photonic structures. The FZP structure allowed all the wavelengths to emerge together towards one focus point; because the structure had a composition of several sized full circles and acted as a lens [18]. However, the CG showed diffracted wavelengths (visible colors) because the structure has multiple semi-circle structures and acted as a grating. The CP structures diffracted different orders in both sides between 5° to 15°; then diffraction became one order on both sides between 20° to 35° (Figure 5b). The rainbow diffraction was measured for all structures from 0° to 35° tilts of SP patterning (Figure 5c).

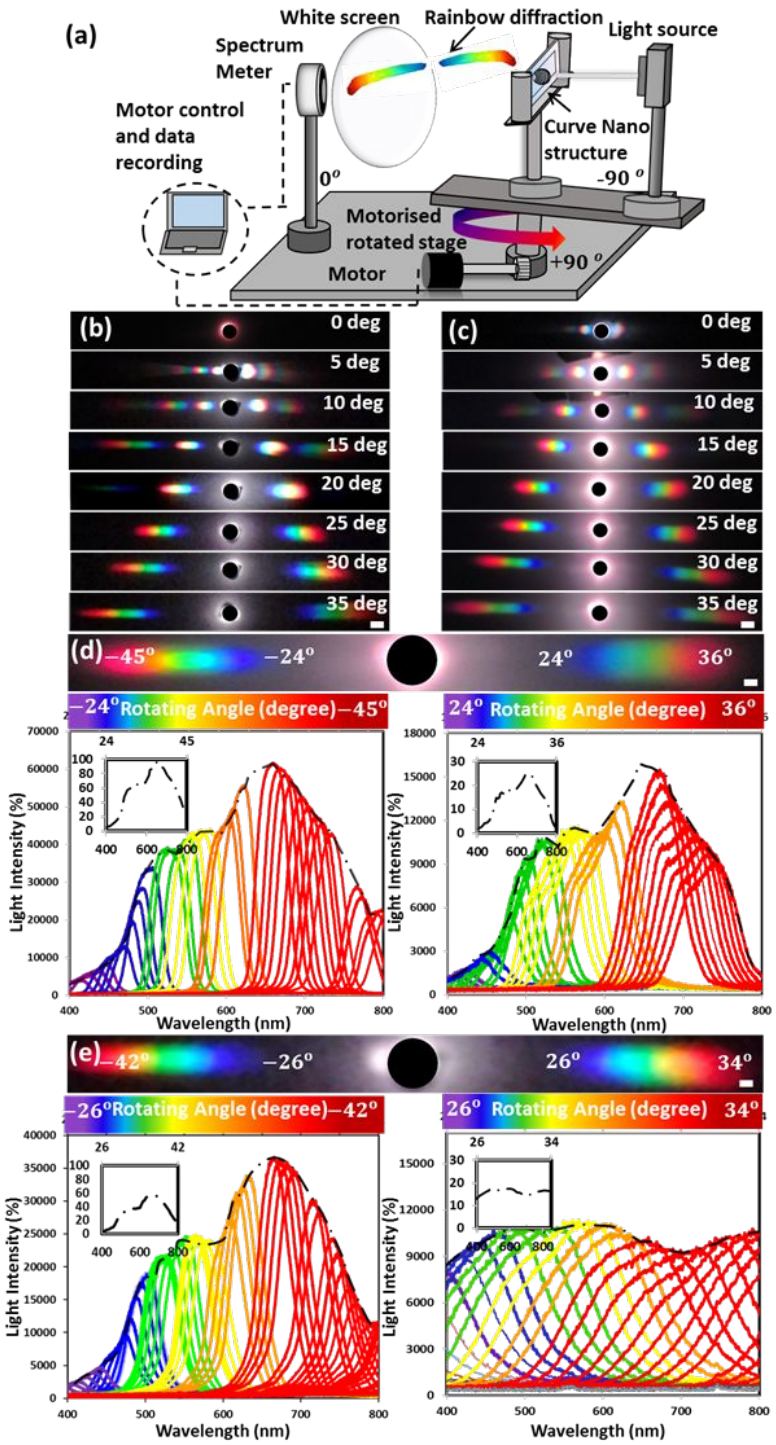

Figure 5. Angle-resolved measurements of structure by fabricated by holographic DLIP. (a) The spectroscopy setup to analyze a broadband white light beam through a sample on a motorized goniometer stage to measure the diffracted rainbow pattern. The rainbow diffraction pattern for (b) CP samples produced at tilt angles of 0° to 35°. (c) SP samples at tilt angles of 0° to 35°. Left and right rainbow diffraction of 25° structure (d) CP pattern, and (e) SP pattern. Scale bar = 1 cm.

The curved photonic structures have more visible wavelength intensity on the left side than the right side due to the curve direction focusing on one side (defocussing on the opposite side). The goniometer set-up was used to analyze the 25° sample produced via CP and SP. The wavelength diffraction profiles were the same on both sides (Figure 5d). The right-side rainbow length was 7.4 cm and the left side was 13.4 cm. On the other hand, the length of the left and right sides of the SP were 5 cm and 10 cm, respectively (Figure 5e). This showed a good focus of the wavelength on one side (right); although the intensity of the SP was less than the CP patterning. This is because the focus point of the SP pattern was shorter than that of the CP pattern due to structural size difference. The FZP, CG, CP and SP structures diffracted all wavelengths. The distribution of the rainbow patterns increased as the structures' size decreased. The CP and SP structures have high wavelength intensity at the right-hand sides due to focussing. The CP structure has a high wavelength intensity because the focus point was at a longer distance than that of the SP pattern.

Applications: curved nanopatterned structure

A low-cost commercial adhesive tape (thickness=100 μm) was used to pattern the photonic structure. Commercial ultra-adhesive tape had several advantages including high strength, flexibility, being waterproof, high transparency, stretchability and resistance to environmental heat [4, 15, 16]. The black dye was deposited on the tape to form a thin film and holographic DLIP was used to generate 1D nanopatterns at a 35° exposure tilt angle (900 nm × 880 nm) (Figure 6a). The 2D structure was designed by a sample rotation of 90° to make the same spacing in the x and y axis (900nm × 880 nm; 900nm × 880 nm) (Figure 6b)[42, 43]. Transmission mode was used to measure the material surface thickness on the tape before and after the nanopatterning process. The broadband halogen light beam was used for transmission analysis with reference

to a plain adhesive tape. The plain adhesive tape showed high light transmission (98%); however, the transmission decreased to 18% after the deposition of the black dye coating.

The transmission increased on the 1D and 2D photonic structures after holographic DLIP patterning. The 2D curved structure showed a higher light transmission than the 1D structure due to more material removal and increased structure gaps (Figure 6c). Hydrophobicity measurement was conducted to measure the change in the tape's surface properties (contact angle) and effects of 1D and 2D nanostructures, respectively (Figure 6d-f). In addition, the three illumination wavelengths were used to display the diffraction from the 2D structure. In addition, the three illumination wavelengths were used to show the wavelength interaction with the 2D structure. They showed an increase in diffraction angle on both axes as the wavelength increased (Figure 6g-i). Moreover, 2D patterns generated two rainbow diffraction spots on both axes (Figure 6j). The RGB room light measurement on a 1D 35° tilt angle structure showed a visible wavelength change from blue to red as the structure was exposed to the light source normally. When the tilt angle of the curved nanostructures was altered from 0.3° to 14.2° at the normal, they displayed visible color changes (Figure 6k). This can add another signal of allowable and critical deformation. Furthermore, the black dye deposited structure was tested in DI water at different pH concentrations to show stability with pH variation (Supporting Information Figure S6). 1D and 2D structures on the clear tape showed changes in transmission and contact angles. Moreover, the 2D structure showed the diffraction angle and rainbow patterns with an extra spot at the y-axis. The 2D structure could help to detect the elongational changes from the two axes. The visible wavelength of the 1D structure based on the changing sample tilt was able to add more information as deflection occurrences. The black dye structure was stable with pH changes to report any of the growth of stalactite straws on a building structure.

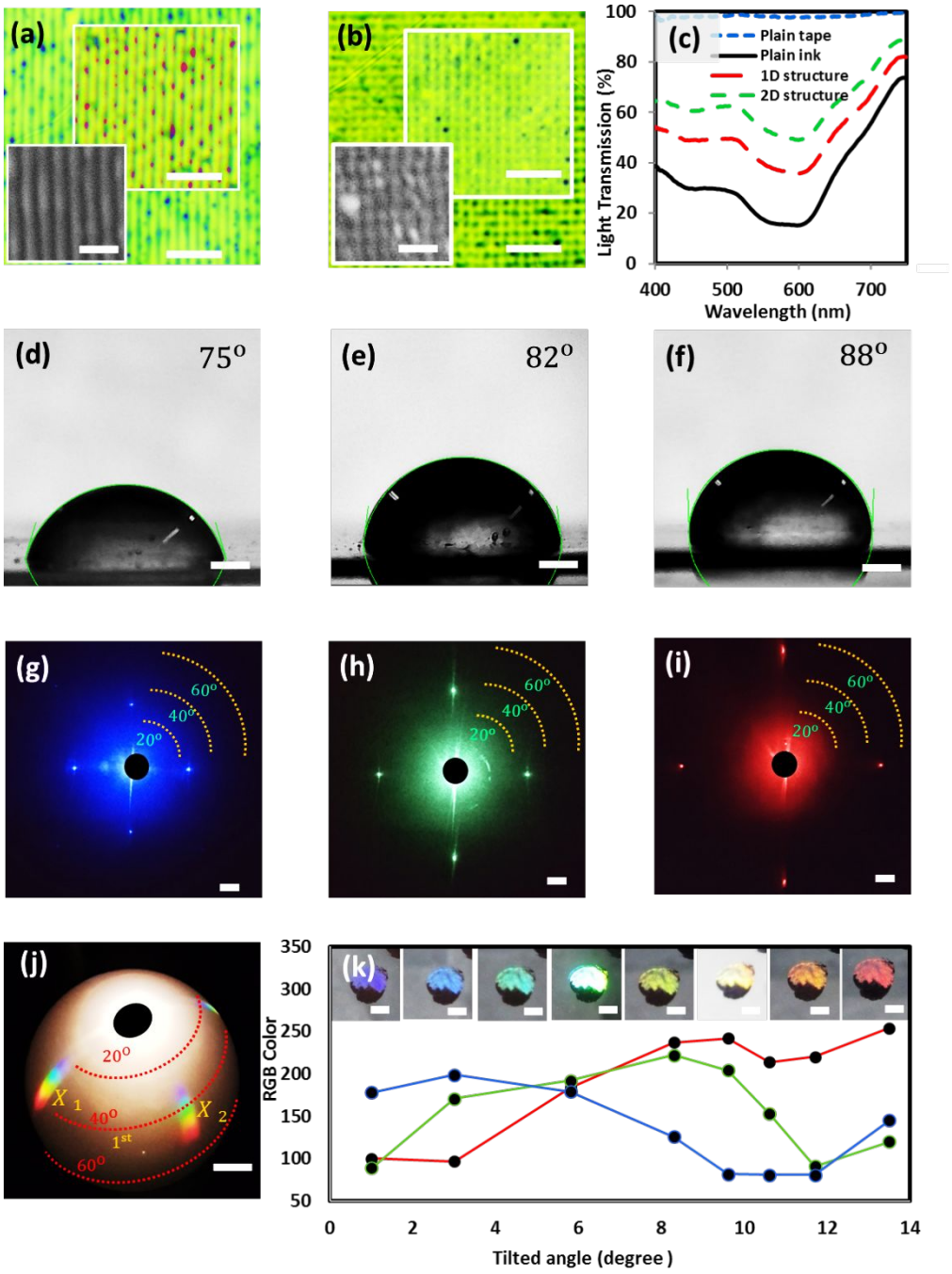

Figure 6. Fabrication of 1D and 2D carved photonic patterns using holographic DLIP. The larger and smaller structure periodicity were(a) 1D (88 nm-900 nm); (b) 2D (900 nm-880 nm × 880 nm × 900 nm); optical microscopy and SEM image scale bar=5 µm, 2 µm ;(c) transmission analysis. Contact angle measurements of (d) plain tape; (e) 1D structure; (f) 2D structure; scale bar = 1 mm; laser illumination of (g) 450 nm; (h) 532 nm; (i) 635 nm. Rainbow diffraction of (j) 2D pattern sample; visible colour analysis of (k) a 1D pattern sample using room (a broadband white) light source. Scale bar = 1 cm.

The 1D SP structure (900 nm × 880 nm) on adhesive tape was used on a tension measurement setup (Figure 7a). The illumination was started with a diffracting angle of 44°. The tape was stretched to analyze the intensity and the diffraction angle variation. The main testing probe measured the diffraction angle on the focused point side. The strain test was conducted on the tape of 4 cm length and 1.5 cm width to measure the Young's modulus of the tape. The tape has ductile behavior (Figure 7b) with an elastic limit of 1.3 N cm^{-2} and Young's modulus of 36.7 N cm^{-2}. Then the tape started to yield in the plastic zone at the Young's modulus of 13.3 N cm^{-2} and 4.6 cm (Figure 7c). The elongation was conducted by stretching the tape with 300 increments of 5 με per stretch, a total of 0.6 cm extension. Seven points were selected to expose the diffraction change positions (Figure 7d). The intensity of diffraction increased as the stretching increased (nonlinear response) because the gap spacing increased to allow more light to focus at a longer distance (Figure 2h-i). The change of diffraction position could measure the change in the elongation. In addition, it allowed the control of the focal length based on tape extension.

Imaging and holographic logo

The CP structure with a 5° tilt angle were used for imaging as the largest structures. The structures would modify efficiently the focal length of the lens (Eq. 7) to create multiple images based on the structure size (Eq. 8) [38, 47].

$$f_{lens}=[1-n]\left(\frac{1}{r_i}-\frac{1}{r_o}\right)\frac{(1-n)d}{r_i r_o n} \quad \text{(Eq.7)}$$

$$f_{img}=\frac{f_{lens}\, r^2}{r^2+2f_{lens}\, mW} \quad \text{(Eq. 8)}$$

where n, r_i, r_o, d represent the lens refractive index, inner radius, outer radius, and lens thickness, respectively. The FZP and CG have shown single images on the zero order (Figure 7e-f). While the 5° of the CP structure showed more than one image. Although, it was supposed to show the focus point on the left of the first order (-1), it showed the main image at zero order

and the first order. This is because the screen was at 15 cm which is out of focus for the first order. The screen was kept in one position to expose the same parameters for all images. In addition, the 5° of the CP structure was exposed to three illumination lasers (Figure 7h-j). Moreover, holographic DLIP with continuous pulses at a sample tilt angle of 35° as used to produce a nanostructured BHAM pattern on the tape. Holographic logo was visualized with room broadband white light and was used as a flexible holographic structure. It can be transferred to other surfaces and it can also be employed for security uses (Figure 7k-m). Additional 2D holographic carved nanostructures were produced with different sizes on the x and y axes. The carved nanostructures have a large structure side for imaging and a small spacing side for sensing (Supporting Information Figure S7).

Radial photonic structures generated by holographic DLIP on an adhesive tape can be used as a conformable strain sensor which can be attached to different surfaces. The intensity of the light diffracted from the curved structure increases as the substrate is stretched to emphasize a strong alert signal during structural damage. The size of the spacing of the curved nanostructure and the length of the tape are the main parameters to increase or decrease the response of the elongation change. The FZP, CG, and 5° of the CP structure were able to provide imaging for the target surface. In addition, the light wavelength could affect the focus distance of the diffraction point for the target object. Moreover, the curved nanostructures could provide a visible sensor under halogen white light. The holographic BHAM curved nanostructure not only displayed a transferable visible commercial logo, but also provided an encrypted light key.

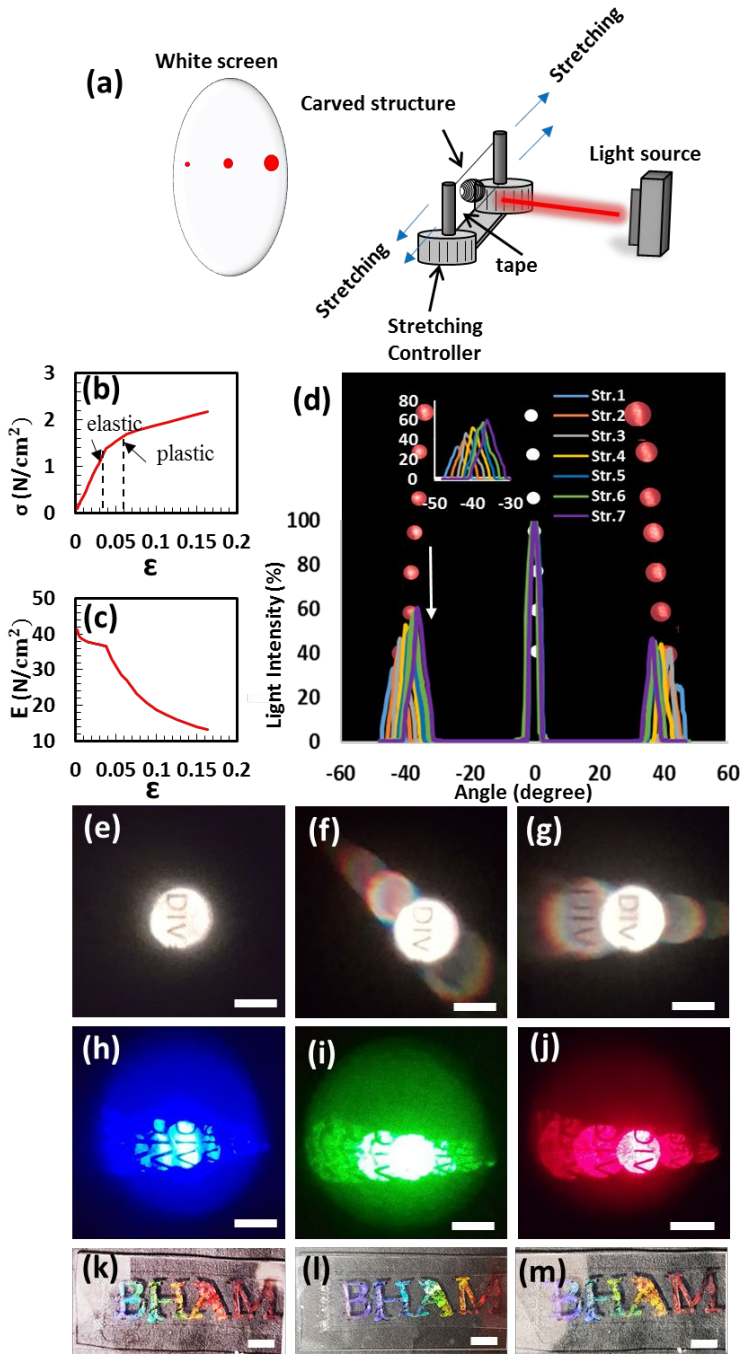

Figure 7. Holographic structure on a tape for elongation measurement and applications. (a) Stretching setup for mechanical measurements of tape. (b) Elastic and plastic deformation. (c) Young's modulus of curved nanopatterns on tape. (d) Stretching diffraction measurement; imaging of the photonic structure by a broadband white light source. (e) Fresnel lens, (f) grating displacement, (g) centre pulse at 5° imaging with monochromatic light through 5° centre pulse structure: (h) 450 nm, (i) 532 nm, (j) 635 nm); holographic curved surface nanograting of (k-m) BHAM logo; scale bar = 1 cm.

Conclusion

Depositing a synthetic black dye on a stretchable tape allowed the formation of nanogratings by a pulsed Nd:YAG laser. The holographic DLIP produced FZP and CG structures and it was able to create different curved structure spacings to behave as a flat lens by changing the sample exposure angle. The spacing and curvature of the structures control the focal length distance. Controlling the curved structure spacing could help to determine the intensity, diffraction, and visual image formation. In addition, adding a lens behind the FZP or large curved structure could help to deliver live images of the targeted structure. The 35° SP nanostructure on the tape was used for measuring the elongation change for strain sensing. The 2D curved structures allowed measuring the surface changes in two axes. A visible color change of the curved structure could add more information and was used to detect structural changes. This pattern could be in the form of a holographic symbol. The black dye nanostructure on the tape was stable in different pH concentrations. The curved structure was able to shape the light intensity as the stretching increased to indicate any significant change (nonlinear response) in geometry. The structures' spacing and the length of the tape are the main parameters that increase or reduce the light signal from any material damage and shifting. The demonstrated curved structures on commercial adhesive tape enabled the sensing of dynamic elongation displayed by holographic images.

Author Contributions

B.A. designed the study and carried out the experiments. H.B., D.B. and A.K.Y. made intellectual contributions and edited the article.

Notes

The authors declare no competing financial interests.

Supporting Information

Diffraction analyses of gratings having different thicknesses in transmission and reflection modes, optical microscopy images of surface grating nanostructures, experimental diffraction analyses of gratings fabricated using a concave mirror, diffraction angle measurement of gratings, holographic 1D nanopatterned structure in response to pH, analyses of 2D patterns produced by holographic DLIP mode

Materials and Methods

Preparation of the recording media of sensing tape:

In the first stage, a black dye (Staedtler Lumocolor) was deposited on a slide glass. Diluted ink solutions (1:8, v/v in ethanol) were spin coated on 1 mm thick glass slides at 200 rpm for 35 s. The dyes used were permanent and had a long-term durability based on manufacturer and from pervious experiments. In the final stage, back dye was deposited on a stronger adhesive tape (Gorilla- crystal clear) on a slide glass. The thickness of the dye on the glass and the tape has been considered based on established work through the transmission mode optical spectra of different spin-coated thicknesses on glass substrates [34].

Fabrication of diffraction gratings on glass and tape

Holographic direct laser interference patterning was used in a Denisyuk reflection mode. A nanosecond pulsed laser (λ = 1064 nm, 180 mJ, 3.5 ns) was used to ablate the black dye deposited on the glass surface and the same on the stretchable tape. The interference between the incident and reflected laser beams ablated localized regions on the dye medium. The exposure angle of all dye films was 0°-35° from the surface of the concave mirror, which was used to produce the object beam in the holography set-up. The concave mirror had a 12.7-mm

diameter; the thickness of the mirror was 3.1 mm at the edge and 3 mm at the deepest point in the centre.

Spectroscopic measurements of the ink gratings

The diffraction of light from 1D and 2D gratings was analyzed by normally illuminating the periodic samples with blue (λ = 450 nm), green (λ = 532 nm), and red (λ = 635 nm) laser beams and recording the transmitted light on a flat screen placed perpendicularly 17 cm away from the sample. The testing was performed on black patterned nanogratings

Angle-resolved measurements of the gratings

A halogen light source (HL-2000, Ocean Optics) with a goniometer set-up was used to achieve angle-resolved measurements of diffraction efficiency on the ink nanogratings. Analysis of the diffracted wavelengths was carried out by placing the sample 17 cm away from the optical probe. A motorized rotating stage was used for the broadband spectroscopic analysis of the rainbow diffraction, which was produced by the nanostructure gratings. The rotation stage had a precision of 0.5° step from the left side 0° to -90° and the right side 0° to +90°.

References

(1) Bekas, D.; Sharif-Khodaei, Z.; Aliabadi, M. H. J. S., An innovative diagnostic film for structural health monitoring of metallic and composite structures. Bekas, D., Sharif-Khodaei, Z. and Aliabadi, M.H., 2018. An Innovative Diagnostic Film for Structural Health Monitoring of Metallic and Composite Structures. Sens. **2018**, 18 (7), 2084.

(2) Zhou, H.; Qin, W.; Yu, Q.; Chen, F.; Yu, X.; Cheng, H.; Wu, H. J. I. J. o. S.; Structures, Controlled Buckling and Postbuckling Behaviors of Thin Film Devices Suspended on an Elastomeric Substrate with Trapezoidal Surface Relief Structures. Int. J. Solids Struct. **2019**, 160, 96-102.

(3) Cardini, A.; DeWolf, J. T. J. S. H. M., Long-term Structural Health Monitoring of a Multi-girder Steel Composite Bridge using Strain Data. Struct. Health Monit. **2009**, 8 (1), 47-58.

(4) Yin, F.; Ye, D.; Zhu, C.; Qiu, L.; Huang, Y., Stretchable, Highly Durable Ternary Nanocomposite Strain Sensor for Structural Health Monitoring of Flexible Aircraft. Sens. **2017**, 17 (11), 2677.

(5) Huang, R. J. J. o. t. M.; Solids, P. o., Kinetic Wrinkling of an Elastic Film on a Viscoelastic Substrate. J. Mech. Phys. Solids **2005**, 53 (1), 63-89.

(6) Smith, G. K., Calcite Straw Stalactites Growing from Concrete Structures. Cave and Karst Sci. **2016**, 43 (1), 4-10.
(7) Yun, H.-B.; Kim, S.-H.; Wu, L.; Lee, J.-J., Development of Inspection Robots for Bridge Cables. Sci. World J. **2013**, (967508), 17.
(8) Campbell, R. A.; Pickett, B. M.; Saponara, V. L.; Dierdorf, D., Thermal Characterization and Flammability of Structural Epoxy Adhesive and Carbon/epoxy Composite with Environmental and Chemical Degradation. J. Adhes. Sci. Technol. **2012**, 26 (7), 889-910.
(9) Kaw, A. K., Mechanics of Composite Materials. 2nd edn (CRC Press, Boca Raton, 2005).
(10) Bocciolone, M.; Bucca, G.; Collina, A.; Comolli, L., Design and Testing of Fibre Bragg Grating Force Transducers for the Measurement of Pantograph–catenary Contact Force. Proceedings of the Institution of Mechanical Engineers, Part F: J. of Rail and Rapid Transit **2018** ,233(4) 396–409.
(11) Trilaksono, A.; Watanabe, N.; Hoshi, H.; Kondo, A.; Iwahori, Y.; Takeda, S., Damage Monitoring in Composite Stiffened Skin using Fiber Bragg Grating under Tensile and Three-point Loading. J Mech Eng Autom **2013**, 3, 227-237.
(12) Trilaksono, A.; Watanabe, N.; Hoshi, H.; Takeda, S. I.; Iwahori, Y., Monitoring Secondary Bending Failure Under Tension Load using Fiber Bragg Grating.. Nanomech. Mater. Struct., Int. Workshop Nanomech. **2012**,18-20.
(13) Huang, Y.; Ding, Y.; Bian, J.; Su, Y.; Zhou, J.; Duan, Y.; Yin, Z., Hyper-stretchable Self-powered Sensors Based on Electrohydrodynamically Printed, Self-similar Piezoelectric Nano/Microfibers. Nano Energy **2017**, 40, 432-439.
(14) Torfs, T.; Sterken, T.; Brebels, S.; Santana, J.; van den Hoven, R.; Spiering, V.; Bertsch, N.; Trapani, D.; Zonta, D., Low Power Wireless Sensor Network for Building Monitoring. IEEE Sens. J. **2013**, 13 (3), 909-915.
(15) Amjadi, M.; Pichitpajongkit, A.; Lee, S.; Ryu, S.; Park, I. J. A. n., Highly Stretchable and Sensitive Strain Sensor Based on Silver Nanowire–elastomer Nanocomposite. ACS nano **2014**, 8 (5), 5154-5163.
(16) Amjadi, M.; Kyung, K. U.; Park, I.; Sitti, M. J. A. F. M., Stretchable, Skin-mountable, and Wearable Strain Sensors and Their Potential Applications: a review. Adv. Funct. Mater. **2016**, 26 (11), 1678-1698.
(17) Rashid, I.; Butt, H.; Yetisen, A. K.; Dlubak, B.; Davies, J. E.; Seneor, P.; Vechhiola, A.; Bouamrane, F.; Xavier, S., Wavelength-Selective Diffraction from Silica Thin-Film Gratings. ACS Photonics **2017**, 4 (10), 2402-2409.
(18) Xu, L.; Rahmani, M.; Kamali, K. Z.; Lamprianidis, A.; Ghirardini, L.; Sautter, J.; Camacho-Morales, R.; Chen, H.; Parry, M.; Staude, I., Boosting Third-harmonic Generation by a Mirror-enhanced Anapole Resonator. Light, Sci. Appl. **2018**, 7, 1-8.
(19) Yu, J.; Zhou, C.; Jia, W.; Ma, J.; Hu, A.; Wu, J.; Wang, S., Distorted Dammann Grating. Opt. Lett. **2013**, 38 (4), 474-476.
(20) Forest, S.; Sievert, R.; Nonlinear Microstrain Theor. Int. J. Solids Struct. **2006**, 43 (24), 7224-7245.
(21) Alqurashi, T.; Alhosani, A.; Dauleh, M.; Yetisen, A. K.; Butt, H., Laser Inscription of Pseudorandom Structures for Microphotonic Diffuser Applications. Nanoscale **2018**, 10 (15), 7095-7107.
(22) Sabouri, A.; Anthony, C. J.; Prewett, P. D.; Bowen, J.; Butt, H., Effects of current on early stages of focused ion beam nano-machining. Mater. Res. Express **2015**, 2 (5), 055005.
(23) Elsherif, M.; HASSAN, M. U.; Yetisen, A. K.; Butt, H., Wearable Contact Lens Biosensors for Continuous Glucose Monitoring using Smartphones. ACS nano **2018**, 12(6), 5452-5462.

(24) Palmer, C. A.; Loewen, E. G., Diffraction Grating Handbook. 2005, Newport Corporation Springfield, Ohio, USA.
(25) Zhang, D.; Zhu, Y.; Liu, L.; Ying, X.; Hsiung, C.-E.; Sougrat, R.; Li, K.; Han, Y., Atomic-resolution Transmission Electron Microscopy of Electron Beam–sensitive Crystalline Materials. Sci. **2018**, 359(6376), 675-679.
(26) Youn, Y.; Ishitsuka, Y.; Jin, C.; Selvin, P. R., Thermal Nanoimprint Lithography for Drift correction in Super-resolution Fluorescence Microscopy. Optics express **2018**, 26 (2), 1670-1680.
(27) Alqurashi, T.; Montelongo, Y.; Penchev, P.; Yetisen, A. K.; Dimov, S.; Butt, H., Correction: Femtosecond Laser Ablation of Transparent Microphotonic Devices and Computer-generated Holograms. Nanoscale **2017**, 9 (39), 15159-15159.
(28) Cavallini, M.; Murgia, M.; Biscarini, F., Patterning a Conjugated Molecular Thin Film at Submicron Scale by Modified Microtransfer Molding. Nano Lett. **2001**, 1 (4), 193-195.
(29) Alqurashi, T.; Penchev, P.; Yetisen, A. K.; Sabouri, A.; Ameen, R. M.; Dimov, S.; Butt, H., Femtosecond Laser Directed Fabrication of Optical Diffusers. RSC Adv. **2017**, 7 (29), 18019-18023.
(30) Leo, K.; Lars Müller-Meskamp; Sylvio Schubert; Teja Roch; Sebastian Eckhardt; Andrés-Fabián Lasagni, Transparent Conductive Metal Thin-Film Electrodes Structured by Direct Laser Interference Patterning. Adv. Eng. Mater.**2015**, 17 (8), 1215-1219.
(31) Q Zhao, A. Y., A Sabouri, SH Yun, H Butt, Printable Nanophotonic Devices via Holographic Laser Ablation. ACS nano **2015**, 9 (9), 9062-9069.
(32) Fernando da Cruz Vasconcellos; Ali K. Yetisen, Y. M.; Haider Butt, A. G.; Colin A. B. Davidson, J. B.; Michael J. Monteiro, T. D. W.; , a. C. R. L., Printable Surface Holograms via Laser Ablation. ACS Photonics **2014**, 1 (6), 489-495.
(33) Zhao, Q.; Yetisen, A. K.; Anthony, C. J.; Fowler, W. R.; Yun, S. H.; Butt, H., Printable Ink Holograms. Appl. Phys. Lett. **2015**, 107 (4), 041115.
(34) AlQattan, B.; Benton, D.; Yetisen, A. K.; Butt, H., Laser Nanopatterning of Colored Ink Thin Films for Photonic Devices. ACS Appl. Mater. Interfaces **2017**, 9(45), 39641-39649.
(35) Vasconcellos, F. d. C.; Yetisen, A. K.; Montelongo, Y.; Butt, H.; Grigore, A.; Davidson, C. A.; Blyth, J.; Monteiro, M. J.; Wilkinson, T. D.; Lowe, C. R., Printable Surface Holograms via Laser Ablation. ACS Photonics **2014**, 1 (6), 489-495.
(36) Aggarwal, M.; Vij, S.; Kant, N., Propagation of Circularly Polarized Quadruple Gaussian Laser Beam in Magnetoplasma. Optik **2015**, 126 (24), 5710-5714.
(37) Zhao, Q.; Yetisen, A. K.; Sabouri, A.; Yun, S. H.; Butt, H., Printable Nanophotonic Devices via Holographic Laser Ablation. ACS nano **2015**, 9 (9), 9062-9069.
(38) Blanchard, P. M.; Greenaway, A. H., Simultaneous Multiplane Imaging with a Distorted Diffraction Grating. Appl. Opt. **1999**, 38 (32), 6692-6699.
(39 Yang, Z.; Zhan, Q., Single-Shot Smartphone-Based Quantitative Phase Imaging Using a Distorted Grating. PloS one **2016**, 11 (7), e0159596.
(40) Naseri, T.; Sadighi-Bonabi, R., Efficient Electromagnetically Induced Phase Grating via Quantum Interference in a Four-level N-type Atomic System. JOSA B **2014**, 31 (10), 2430-2437.
(41) Hecht, E.; Zajac, A., Optics Addison-Wesley. Reading, Mass **1974**, 19872, 350-351.
(42) AlQattan, B.; Butt, H.; Sabouri, A.; Yetisen, A. K.; Ahmed, R.; Mahmoodi, N., Holographic Direct Pulsed Laser Writing of Two-dimensional Nanostructures. RSC Adv. **2016**, 6 (112), 111269.
(43) AlQattan, B.; Yetisen, A. K.; Butt, H., Direct Laser Writing of Nanophotonic Structures on Contact Lenses. ACS nano **2018**, 12(6), 5130-5140.
(44) Blanchard, P. M.; Fisher, D. J.; Woods, S. C.; Greenaway, A. H., Phase-diversity Wave-front Sensing with a Distorted Diffraction Grating. Appl. Opt. **2000**, 39 (35), 6649-6655.

(45) Deng, S.; Yetisen, A. K.; Jiang, K.; Butt, H., Computational Modelling of a Graphene Fresnel Lens on Different Substrates. RSC Adv. **2014**, 4 (57), 30050-30058.
(46) Deng, S.; Penchev, P.; Liu, J.; Wang, Y.; Jiang, K.; Dimov, S.; Zhang, Z.; Liu, Y.; Leng, J.; Butt, H., Laser Directed Writing of Flat Lenses on Buckypaper. Nanoscale **2015**, 7 (29), 12405-12410.
(47) Blanchard, P.; Greenaway, A., Broadband Simultaneous Multiplane Imaging. Opt. Commun. **2000**, 183 (1-4), 29-36.

TOC

90x33mm (150 x 150 DPI)